Polym. Bull. (2018) 75:1487–1504
https://doi.org/10.1007/s00289-017-2096-x

ORIGINAL PAPER

Fabrication and characterization of chitosan/gelatin/nanodiopside composite scaffolds for tissue engineering application

Abbas Teimouri[1] · Shahin Roohafza[1] · Mohammad Azadi[1] · Alireza Najafi Chermahini[2]

Received: 11 March 2017 / Revised: 2 May 2017 / Accepted: 12 June 2017 /
Published online: 28 June 2017

Abstract Composite scaffolds were prepared from the mixture of chitosan (C), gelatin (G) and nanodiopside (nDP) in different inorganic/organic weight ratios using the freeze-drying method. The prepared nDP and composite scaffolds were investigated using BET, FT-IR, SEM and XRD techniques. The composite scaffolds had 70–81% porosities with interlinked porous networks. Moreover, investigation of the cell proliferation, adhesion and viability using MTT test and mouse pre-osteoblast cell proved the cytocompatible nature of the composite scaffolds with improved cell attachment and proliferation. All these results essentially illustrated that this composite could have a potential ability for the tissue engineering applications.

Keywords Chitosan · Gelatin · Nanodiopside · Composite scaffold · Tissue engineering

Introduction

The tissue engineering approach is encouraging as it can mend or renew the injured tissue through the replacement by the engineered tissue, to reconstruct the functions during revival and then, to join with the host tissue. In this regard, important consideration is being given to three-dimensional (3-D) polymer scaffolds for tissue engineering applications [1, 2]. These scaffolds supply the vital support as artificial additional cellular matrices, permitting cells to proliferate and preserve their

✉ Abbas Teimouri
a_teimouri@pnu.ac.ir; a_teimoory@yahoo.com

[1] Department of Chemistry, Payame Noor University (PNU), P.O. Box 81395-671, Tehran 19395-3697, Iran

[2] Department of Chemistry, Isfahan University of Technology, Isfahan 841543111, Iran

discriminate acts. A perfect scaffold should imitate the natural extracellular environment of the tissue to be regenerated. Scaffolds mimicking the natural extracellular environment could have much biocompatibility.

In the bone tissue, the extracellular matrix comprises an organic phase composed of type I and type III collagen and glycosaminoglycans (GAGs) and an inorganic phase made up of hydroxyapatite (HA) [3].

Chitosan is a partially deacetylated product made from chitin and is structurally similar to glycosaminoglycans [4]. Chitosan is biocompatible and can be broken down by enzymes in the body and the resulting products are non-toxic. Chitosan is greatly used in tissue engineering because of its many advantages, like hemostasis in injure curing, fast tissue regeneration and antibacterial characteristics [5–9]. Chitosan can be shaped into different forms and can become a porous structure by freeze drying. However, its bioactivity needs to be improved, like most polymers, by the addition of biologically active materials such as diopside, hydroxyapatite, collagen, or gelatin [10].

Gelatin is a partly broken-down product of collagen. Collagen possesses antigenicity because of its animal parentage; however, gelatin has comparatively low antigenicity, in contrast to its precursor; yet it still keeps some data signals which may promote cell attachment, differentiation and proliferation, such as the Arg–Gly Asp (RGD) order of collagen [11]. Gelatin has been mixed into chitosan scaffolds to promote cell adhesion, migration, differentiation and proliferation [12, 13]. Some studies on the applications of chitosan and gelatin in bone tissue engineering applications are shown in Table 1.

Diopside powders and dense ceramics have been shown to be bioactive materials for bone regenerations in biomaterial science [19]. The advantages of these ceramics in bone tissue regeneration, as compared to HA and other ceramic scaffolds, have been reported; among them, diopside with the chemical formula of $CaMgSi_2O_6$, both in powder or bulk form, possesses a lower degradation speed and has the ability of in vitro apatite formation and in vivo bone regeneration. It has been reported that surface roughness, micro and nanotopography can influence cell morphology, cell expansion, cytoskeletal reorganization, cell proliferation and differentiation. In addition, it is recognized that the degradation products of diopside in physiologic fluids, such as silicon, calcium, and magnesium, could promote the proliferation and differentiation of osteoblast cells [20]. Mg ions are mainly responsible for the apatite formation ability of the scaffolds, and Si ions are able to stimulate cell growth and differentiation on the scaffolds. Therefore, diopside is considered to be an attractive material for bone tissue engineering applications [21]. Various methods have been demonstrated that mechanical properties of diopside, specifically bending strength and fracture toughness, are significantly higher than those of HA making it suitable for bone tissue engineering application [22–24]. Nonami and Tsutsumi have shown that diopside bioceramic not only has no toxicity symptom after implantation in the bones of rabbits and monkeys, but also could bond with host bone [25].

Studies have shown that composite scaffolds of chitosan with nanohydroxyapatite improve the osteoblast and fibroblast cell viability [26–28]. Also, hydroxyapatite/Al_2O_3/diopside scaffold and other multi-component scaffolds and their

Table 1 Some studies on CG-based systems for bone tissue engineering applications

Scaffold content	Preparation method	In vitro testing		References
		Mechanical properties	Cell culture studies on scaffold	
Hydroxyapatite/chitosan–gelatin	Blending	–	Good attachment and biocompatible	[14]
Gelatin–chitosan–nanobioglass	Freeze-drying	Maximum compressive strength of 2.2 ± 0.1 MPa	High cellular activity	[15]
Chitosan–gelatin/nanohydroxyapatite	Freeze-drying	Increased tensile strength	High cell attachment and high cell viability	[16]
Chitosan–gelatin/β-tricalcium phosphate	Lyophilizing	Compressive properties were improved, especially compressive modulus from 3.9 to 10.9 MPa	Good biocompatibility and mild inflammatory response	[17]
Chitosan/gelatin/nano hydrxyapatite	Blending	–	High proliferation and differentiation	[18]
CG/nDP	Freeze-drying	Maximum compressive strength of 2.9 ± 0.05 MPa	High cell attachment and high cell viability	This work

properties have been investigated by comparing them with bi-component scaffolds [29, 30]. However, the influence of nDP on CG composite scaffolds is not well understood. In the continuation of our recent studies on the construction of composite scaffolds [31–36], in this work, we have focused on the preparation, characterization, bioactivity, biodegradation and in vitro properties of nanocomposite scaffolds CG/nDP in detail. The aim of this study is to prepare porous composite scaffolds, evaluate their physical (pore structure mechanical strength and mechanical stability), chemical (degradation and apatite formation) and biological (cell morphology and proliferation) properties and explore their potential application in tissue engineering.

Experimental

Materials

Chitosan powder (low molecular weight, 85% deacetylated) was bought from Sigma-Aldrich, USA. Gelatin was purchased from Merck. Calcium nitrate

tetrahydrate, glutaraldehyde, magnesium chloride hexahydrate and tetraethyl orthosilicate (TEOS) were bought from Sigma-Aldrich. For the in vitro study of cytotoxicity, a mouse preosteoblast cell line (MC_3T_3-E_1) was provided by Riken Cell Bank (Ibaraki, Japan). The MC_3T_3-E_1 cells were cultured with low glucose-Dulbecco's modified Eagle's medium (DMEM), which contained 10% fetal bovine serum and 1% penicillin–streptomycin (GIBCO, Gaithersburg, MD, USA) in a humidified 37 °C incubator with 95% air and 5% CO_2. Ascorbic acid and 3-(4,5-dimethylthiazol-2-yl)-2,5-diphenyltetrazoliumbromide (MTT) were supplied from Amersco Co. (Solon, OH, USA). Fetal bovine serum (FBS) solution was bought from Gibco, Invitrogen Corporation. Acetic acid and all other solvents and chemicals were purchased from Merck.

Methods

Preparation of nDP

nDP was synthesized by the modified sol–gel method [37]. In short, we dissolved 0.125 mol of $Ca(NO_3)_2{\cdot}4H_2O$ and $MgCl_2{\cdot}6H_2O$ in pure ethanol and stirred it forcefully in reflux for 30 min at 80 °C to dissolve these precursors in the solvent. TEOS was added to the homogeneous solution and slowly stirred to convert it to a wet gel. Drying in an oven at 100 °C for 24 h resulted in a dried powder, ground in a hand-mortar; then it was calcined at 700 °C for 2 h, and 1100 °C for 1 h. The resultant nDP was powdered using mortar and pestle to reduce its size. Finally, it was ball-milled in a zirconia mechanical ball mill for 8 h to furnish diopside nanopowder.

Preparation of composite scaffolds

Chitosan 2% (w/v) was dissolved in 1% acetic acid solution at 37 °C. Gelatin 5% (w/v) was dissolved in deionized water at 50 °C, added into chitosan solution and stirred for 24 h at 37 °C. Then, nDP was added to the solutions and stirred for 48 h to scatter nDP in the chitosan/gelatin solution. The resultant solution was subjected to ultrasonication to further scatter and decrease particle size. 0.25% glutaraldehyde was added as a cross-linker. The resultant solution was transferred to 24-well culture plates and pre-freezed at −20 °C for 12 h; this was followed by lyophilization at −80 °C for 14 h. Then, the scaffolds were stored for further use. The nDP content of each specimen was scaled according to the CG/nDP weight ratios of 100/0, 80/20, 70/30 and 60/40, as listed in Table 2.

Characterizations

The morphologies of the synthesized samples were evaluated by scanning electron microscopy (SEM), using a Philips XL30 at an acceleration voltage of 20 kV. In addition, the samples were analyzed by X-ray diffraction (XRD) using a Philips X'PERT MPD X-ray Diffractometer (XRD) with Cu Kα radiation

Table 2 Characteristics of CG/nDP composites

CG/nDP composition (wt/wt)	Characteristics of the composite scaffolds		
	Water absorption (%)	Scaffold surface/volume ratio (mm^2/mm^3)	Pore size (μm)
100/0	1363 ± 201	269.18 ± 21	146 ± 39
80/20	9093 ± 128	290.73 ± 25	113 ± 33
70/30	11,054 ± 235	301.69 ± 18	103 ± 37
60/40	11,968 ± 197	311.34 ± 20	95 ± 29

Values are mean ± SD ($n = 5$). Significant difference ($p \leq 0.05$)

($\lambda = 0.154056$ nm). The XRD patterns were recorded in the 2θ angle range of 10°–100°. A JASCO FT/IR-680 PLUS spectrometer was used to record the FT-IR spectra using KBr disks. The Brunauer–Emmett–Teller (BET) specific surface areas and Barrett–Joyner–Halenda (BJH) pore size distribution of the samples were determined by adsorption–desorption of nitrogen at liquid nitrogen temperature, using a series BEL SORP 18.

Water absorption (%)

For water uptake measurements, all the specimens were weighed before being immersed in distilled water at 37 °C [38]. After immersion for different periods, the samples were carefully removed from the media and gently pressed in-between two filter papers to remove the excess water and finally weighed using a sensitive balance. The water absorption ability (%) can be calculated by the following equation:

$$\text{Water absorption } (\%) = [(W_W - W_0)/W_0] \times 100,$$

where W_0 is the initial weight of the sample, and W_W is the sample weight after immersion. The test was carried out for five samples, and the average value was taken to insure the data. Values are mean ± SD ($n = 5$).

Mechanical properties

Mechanical properties, including compressive strength and modulus of the samples, were measured in the dry state at a crosshead speed of 2 mm/min in a material prufung 1446-60 machine (Zwick). The samples with size of 1 × 1 × 1 cm were used in the compressive property test.

Porosity analysis

Liquid displacement method was used to measure the porosity of scaffolds. The procedure was as follows: first, the volume and weight of the scaffolds were measured, noted as V and W_d, respectively. Secondly, the sample was immersed into

the water in vacuum (5 min) and taken out and was weighed again and noted as W_w. Finally, the porosity of the scaffold, ε, was evaluated using:

$$\varepsilon = \frac{W_w - W_d}{\rho V}.$$

The volume of the scaffolds was measured based on the following formula:

$$V = \pi \times \left(\frac{D}{2}\right)^2 \times H,$$

where ρ is the density of water (1000 g/cm^3), π is the pi-constant (value = 3.1415), D is the diameter, and H is the height of the scaffold. Values are mean ± SD ($n = 5$).

Surface hydrophilicity

Surface hydrophilicity was evaluated by measuring the water contact angles of the cast discs of CG/nDP suspension through a drop shape analysis system (DSA100M, Kruss, Hamburg, Germany).

In vitro biodegradation

The degradation of the composite scaffolds was investigated in a phosphate buffer saline (PBS) solution at pH 7.4 and room temperature. Three scaffolds were submerged in the PBS buffer for 1, 3, 7 and 14 days. The initial weight of the scaffold was written as W_0, and after 1, 3, 7 and 14 days, the scaffolds were rinsed in deionised water to clean ions adsorbed on their surface and then, they were put in the oven to be dried at 30 °C for 24 h. The dry weight was written as W_t. The degradation of the scaffold was computed using the sub formula:

$$\text{Degradation } (\%) = [(W_0 - W_t)/W_0] \times 100.$$

Degradation rate was imparted as mean ± SD ($n = 3$).

In vitro biomineralization

Three composite scaffolds of distinct weight were investigated in the simulated body fluid (SBF) solution (pH 7.40) at 37 °C [39], within a closed falcon tube for 7 and 14 days, and then the scaffolds were put in the oven to be dried at 30 °C for 24 h. Then, they were freeze-dried, sectioned and viewed using SEM, XRD and FT-IR for mineralization.

MTT assay

The MTT assay was carried out for cell viability and mitochondrial activity assessment [40]. Living cells reduced the MTT substrate (3-[4,5-dimethylthiazol-2-

yl]-2,5-diphenyltetrasodium bromide) to a dark-blue formazan in the presence of active mitochondria and, thus, an accurate measure of mitochondrial activity of cells in a culture was carried out. 2×10^5 cells/cm^2 were seeded in scaffolds and cultured in 24-well plates for 24, 48 and 72 h. As positive control, Triton X-100 (0.1%) was added to the wells containing cells. The negative control included the cells seeded into the wells with the regular medium. Incubation was carried out for 24 h. The exhausted culture medium was replaced with some 400 µl fresh culture medium containing 40 µl MTT solution (MTT, Sigma, USA) (5 mg ml^{-1}) in each well; this was followed by incubation for 4 h at 37 °C. After incubation, 400 µl of dimethyl sulfoxide (Sigma, USA) was added to dissolve the blue formazan crystals and 100 µl of the solution was transferred to the 24-well plate; also, absorbance was measured at 570 nm in an ELISA reader (Hyperion MPR4). To observe adhesion and morphologies of the cells attached to the scaffolds, the cells were rinsed with PBS and then soaking was done with 2.5% glutaraldehyde in PBS solution for 1 h at room temperature. After soaking, the cells were dehydrated in a graded series of ethanol aqueous solutions (70–100%) and dried in vacuum at room temperature.

Statistical analysis

Statistical analyses were carried out by SPSS v.16.0 software. Data were denoted as the mean ± significant when p values obtained from the test were less than 0.05 ($p < 0.05$).

Results and discussion

Scaffold characterization

SEM analysis

The nDP particles filled the pores of the composite scaffold and were dispersed in the matrix (Fig. 1). The pore size of CG and CG/nDP composite scaffold varied from 150 to 350 µm, as assessed by SEM (Fig. 1). Although the pore size of CG/nDP scaffolds was decreased with the addition of nDP, as compared with the CG scaffold, the results were not statistically important. However, with the increasing concentration of nDP, the pore sizes were decreased.

XRD analysis

The XRD spectra (Fig. 2a) show diffraction peaks at about 27°, 28°, 31°, 33°, 36° which represents the XRD pattern of prepared crystallized diopside ($CaMgSi_2O_6$: ICDD card: 78-1390). Critical calcination temperature of 1100 °C was obviously ideal to obtain pure diopside with no impurity of other ceramics. It yielded strong diopside peaks at about (220), (221), (310), (311) and (131) planes [31, 37]. The XRD of CG/nDP scaffold exhibits peaks at 30° and 35° ascribed to the presence of nDP in the composite scaffold, which was not present in CG scaffold (Fig. 2b). In

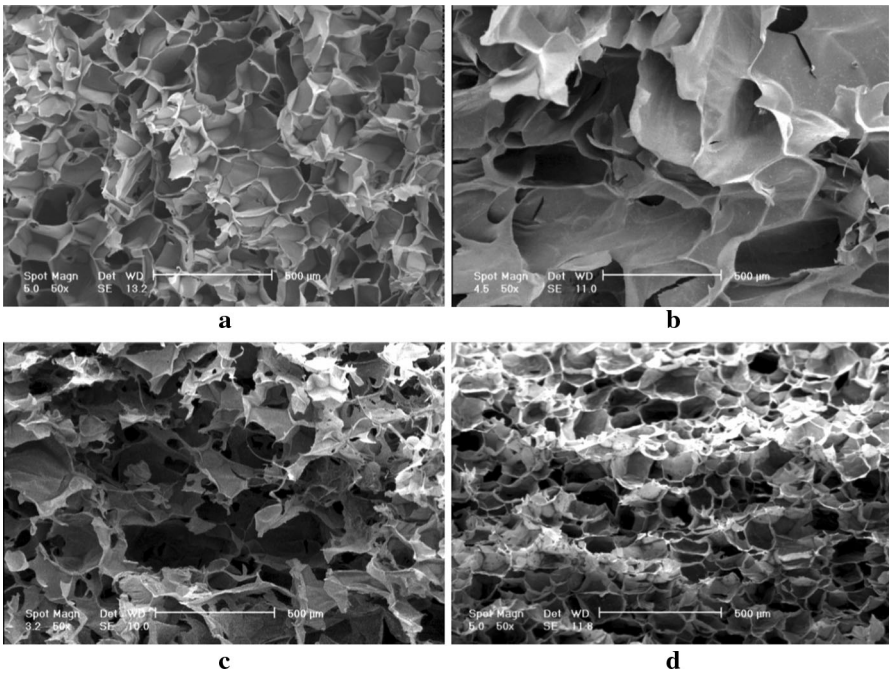

Fig. 1 SEM images of **a** CG scaffold, **b** 80/20 composite, **c** 70/30 composite, and **d** 60/40 composite

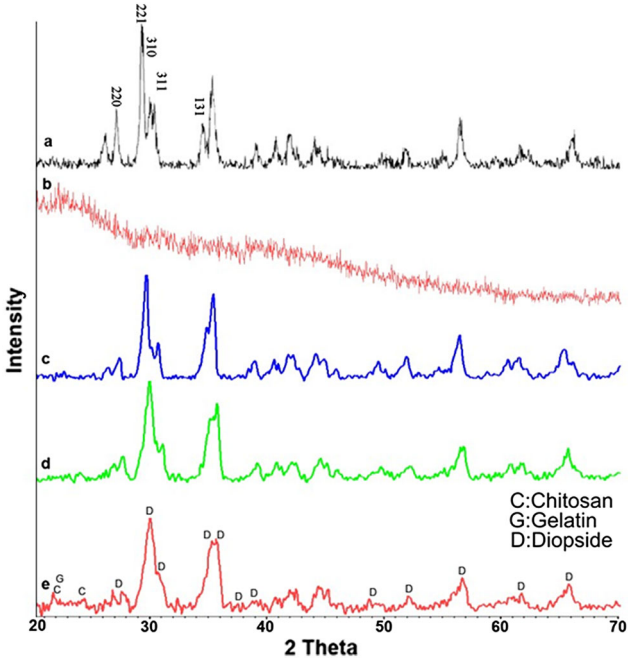

Fig. 2 XRD patterns of *a* pure nDP, *b* CG scaffold, *c* 80/20 composite, *d* 70/30 composite, and *e* 60/40 composite

40% nDP incorporated scaffold, the peaks had intensities less than the higher concentration of nDP (Fig. 2c–e). The decrease in the intensity was owing to the interaction of CG with the nDP.

FT-IR analysis

FT-IR spectrum of nDP (Fig. 3a) exhibited peaks in the area 650 cm^{-1} that corresponded to the bending vibrations, and the peaks in the area 900–1100 cm^{-1} referred to the stretching vibrations of the silicate structure. The FT-IR spectra of gelatin indicated peaks at 3423 and 3174 cm^{-1} due to –NH stretching of the secondary amide, C–H stretching at 2922 and 2850 cm^{-1}, C=O stretching at 1643 cm^{-1}, –NH bending at 1545 cm^{-1}, and –NH out of-plane wagging at

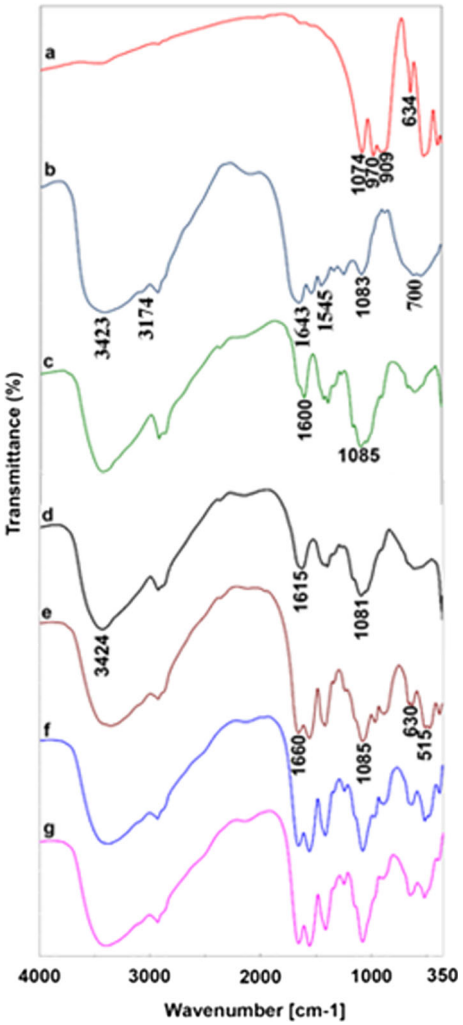

Fig. 3 FT-IR spectra of *a* pure nDP, *b* pure G, *c* pure C, *d* CG scaffold, *e* composite 80/20, *f* composite 70/30, and *g* composite 60/40

700 cm^{-1} (Fig. 3b). FT-IR spectra of C (Fig. 3c) exhibited a peak at 1600 cm^{-1} that corresponded to the primary amide groups of chitosan. The peak at 1085 cm^{-1} was allocated to the C–O stretching of chitosan. Comparing the FT-IR spectra of CG (Fig. 3d) with CG/nDP (Fig. 3e–g) implied that distinctive peaks of nDP, chitosan and gelatin existed in the composite scaffolds. In analogy to CG, CG/nDP composite scaffold varied by two new absorption peaks at 618 and 560 cm^{-1}, corresponding to the bending vibration peaks of the silicate structure. FT-IR studies revealed that there was a stronger interaction between nDP and CG networks in the scaffold. The –COOH groups of gelatin in the composite scaffold exist in the form of COO^- and the ionic or polar interaction could be between COO^- and Ca^{2+}. Hydrogen bonds could also exist between $–NH_2$ groups of chitosan and oxygen of Si–O–Si groups of nDP (Fig. 4) [41–43].

BET analysis

One of the most important methods used to accurately measure the total surface area of porous samples is the BET method, while the BJH method is often used in calculating the pore size. The nitrogen adsorption/desorption isotherm and the pore size distribution (inset) are shown in Fig. 5. The surface area and pore volume of the CG/nDP were found to be 10.084 m^2/g and 0.096 cm^3/g, respectively. As shown in Fig. 5, an open loop adsorption–desorption isotherm was observed for the composite. This observation provided important information about the structure of this composite material. Generally, occurrence of an open loop BET diagram is attributed to chemisorption of N_2, where the vacant sites are not the same as the occupied ones. It may also be found in certain situations in which the mechanism of mesopore filling by capillary condensation varies from mesopore emptying. Moreover, the hysteresis may arise from the occurrence of irreversible capillary condensation within the well-defined mesopores. The isotherm can be assigned to a Type II isotherm, corresponding to non-porous or macroporous materials. The hysteresis loops of Type H3, according to IUPAC classification, typically occur at $P/P_0 > 0.5$, which is not in the normal BET range. Furthermore, the type of hysteresis loops observed in these isotherms indicated that they were most likely due to the slit-shaped pores.

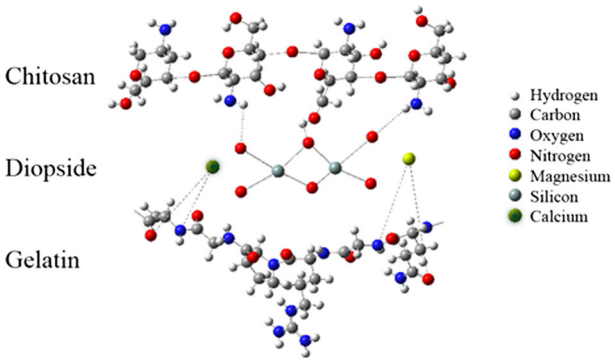

Fig. 4 The interactions between the C and G network and nDP in (CG/nDP) composite scaffolds

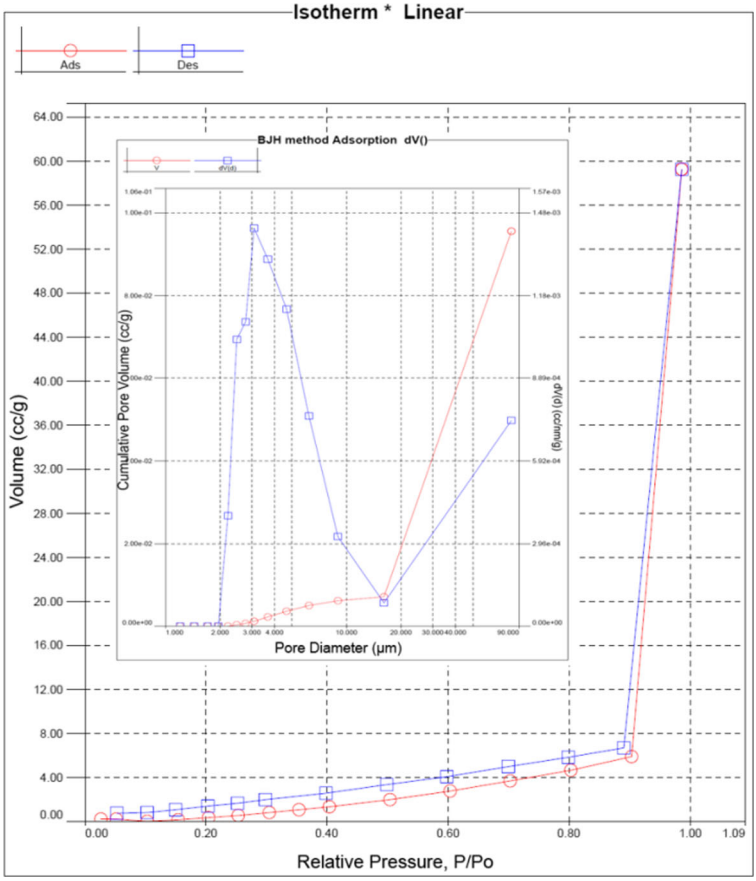

Fig. 5 N_2 adsorption–desorption isotherm and the pore size distribution (*inset*) of composite 80/20

Water absorption (%)

To evaluate the biomaterial for tissue engineering, hydrophilicity of the CG polymer matrix is one of the most critical features considered for the absorption of body fluid and transfer of cell nutrients and metabolites. Water absorption ability ratio was constantly increased with increasing the concentration of nDP, especially the 60/40 composite (Table 2). The observed results were due to the ability of CG polymeric matrix to form the reversible gel; its increasing pressure in the mixture of CG/nDP lowered the weight fractions of nDP in it. In this way, a lower degree of crystallinity enhanced water absorption ability of the 60/40 composite. In this study, gelatin had positive effects on cell adhesion, viability, and growth. Moreover, the incorporation of gelatin with chitosan improved the hydrophilicity of chitosan membranes and the hydrophilic surface was more suitable for cell attachment and proliferation.

Mechanical properties

The composite scaffolds must have sufficient porosity for cell proliferation, but they should also provide good mechanical strength to support the frame during tissue regeneration. The tenacity of the composite scaffolds was compared according to the amount of nDP. In this work, the effect of the nDP incorporation on the compressive strength and compressive modulus (Table 3) of the composite scaffolds was studied. The increase in pore wall thickness and the reduction in pore sizes by the addition of nDP could be a reason for the suitable mechanical properties in the composite scaffolds, in comparison to the CG scaffolds. However, while the water uptake of scaffolds would enhance cell adhesion, it could lower its mechanical properties.

Porosity

The presence of nDP in CG scaffolds caused reduction in porosity (Table 4). Porosity is a measure of permeability which facilitates diffusion of nutrients and cytokines into the scaffold and the removal of waste products from it. However, it should be noted that an increase in porosity can weaken the scaffold for tissue engineering. Some studies on the porosity of different composite scaffolds containing CG or DP in tissue engineering applications are shown in Table 5.

Surface hydrophilicity

Surface hydrophilicity helps the storage of growth factors and transportation of the wastes and nutrients in both native tissues and scaffolds [31]. The mean values of water contact angles are presented in Table 4. It is obvious that the composite scaffolds have better hydrophilicity compared to the CG scaffold. The presence of

Table 3 Summary of mechanical properties of CG/nDP composites

CG/nDP composition (wt/wt)	Compressive strength (MPa)	Compressive modulus (MPa)
100/0	0.9 ± 0.06	51 ± 5.05
80/20	1.6 ± 0.04	67 ± 10.12
70/30	2.1 ± 0.02	115 ± 11.09
60/40	2.9 ± 0.05	168 ± 12.07

Values are mean ± SD ($n = 5$). Significant difference ($p \leq 0.05$)

Table 4 Porosity and water contact angles of CG/nDP composites

CG/nDP composition (wt/wt)	Porosity	Water contact angle (°)
100/0	78.00 ± 3.10	92.29 ± 5.71
80/20	72.00 ± 1.15	83.05 ± 2.90
70/30	65.00 ± 2.05	76.30 ± 3.05
60/40	58.00 ± 2.48	65.29 ± 5.21

Values are mean ± SD ($n = 5$)

Table 5 Porosity of different composite scaffolds containing CG or DP

Composite	Method	Porosity (vol.%)	References
Chitosan–gelatin/β-tricalcium phosphate	Freezing and lyophilizing	92–98	[15]
Gelatin–chitosan-nanobioglass	Freeze-drying	More than 80	[17]
Poly(ε-caprolactone)/diopside	Electrospinning	59.77–70.1	[24]
Diopside/silk fibroin	Freeze-drying	69–85.7	[31]
Chitosan/nanodiopside/nanohydroxyapatite	Freeze-drying	50–85	[41]
β-Chitin/nanodiopside/nanohydroxyapatite	Freeze-drying	50–75	[42]
CG/nDP	Freeze-drying	70–81	This work

diopside nanoparticles in the CG scaffolds showed an effective rout toward the modification of CG hydrophobicity and makes the surfaces of the scaffolds favorable to the growth of the attached cells in tissue engineering applications.

In vitro biodegradation studies

The degradation conduct of scaffolds in the normal PBS solution (Fig. 6), upon analysis, presented a pronounced degradation pattern for all scaffolds. CG scaffold showed a higher degradation rate in the PBS solution. This could be ascribed to an increase in the hydrophilicity of the composite. But, the degradation rate of the composite scaffolds was decreased with the addition of nDP into the matrix. The union of nDP significantly decreased the degradation rate with around 35% of nanocomposite still remaining after 28 days. This shows that the degradation of the composite scaffold could be modified by the addition of nDP. A scaffold's capacity to degrade in concert with the new tissue formation is a main parameter in scaffold design for tissue regeneration.

In vitro biomineralization studies

The scaffolds showed an excellent ability to undergo mineralization in the SBF solution at the physiological pH and temperature. The presence of mineralization

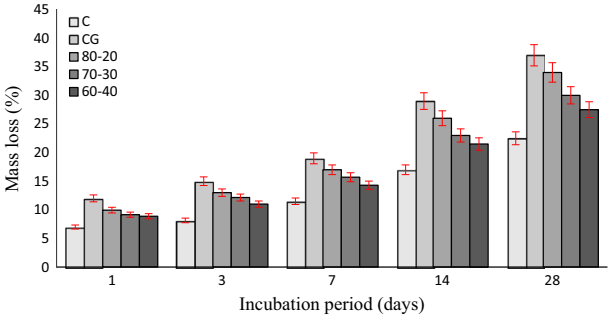

Fig. 6 Degradation behavior vs time curve of scaffolds in PBS at 37 °C

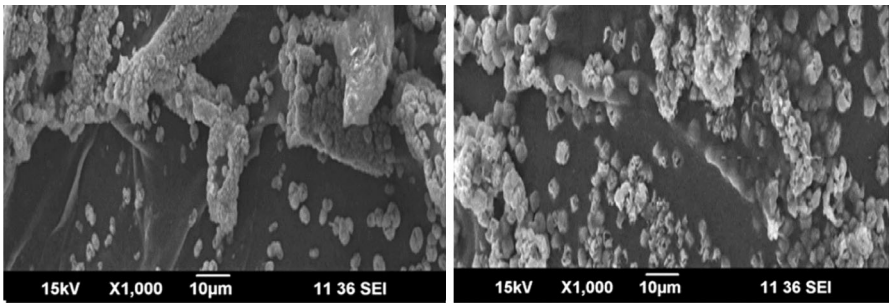

Fig. 7 SEM images of **a** composite 80/20, after soaking in SBF solution for 7 days and **b** after 14 days

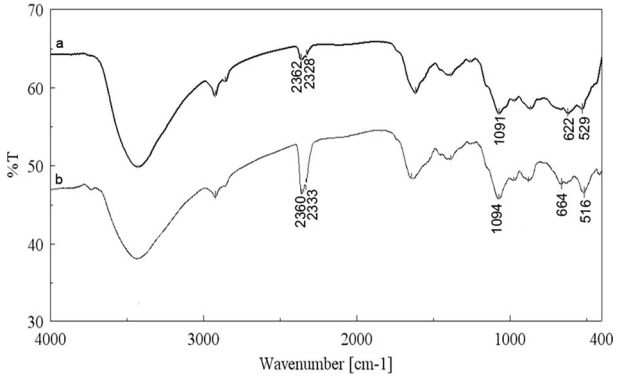

Fig. 8 FT-IR spectra of *a* composite 80/20, after soaking in SBF solution for 7 days and *b* after 14 days

was observed qualitatively through SEM (Fig. 7), FT-IR (Fig. 8) and XRD (Fig. 9) analysis, all showing an increase in hydroxyapatite deposition in the nanocomposite, within 7–14 days of incubation in the SBF solution. It has been reported that that in nDP containing composites, hydrolysis of nDP network leads to the formation of Si–OH groups which provide favorable sites for apatite nucleation. The negatively charged Si–OH groups electrostatically interact with positively charged calcium ions, forming an amorphous calcium silicate which further interacts electrostatically with negatively charged phosphate ions, which, in turn, form an amorphous calcium phosphate. These precursors of apatite then grow by consuming calcium and phosphate ions from the surrounding fluid [41–47].

In vitro evaluation of cytotoxicity and cell attachment studies

Cytocompatibility of the CG/nDP nanocomposite scaffolds was assessed using the MTT assay. The results proposed that there were no significant toxic leachates in the CG/nDP scaffolds after the incubation of the cells with the extract containing the leachates obtained after 24, 48 and 72 h of incubation in the medium (Fig. 10). No significant increase in cell growth was seen in the control, CG groups after culturing for 72 h due to the space deficiency in the multi-well culture dishes, but the cells

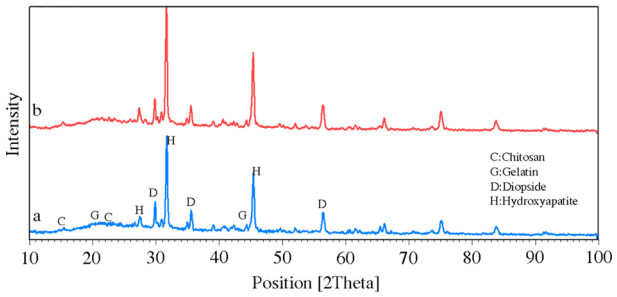

Fig. 9 XRD patterns of *a* composite 80/20, after soaking in SBF solution for 7 days and *b* after 14 days

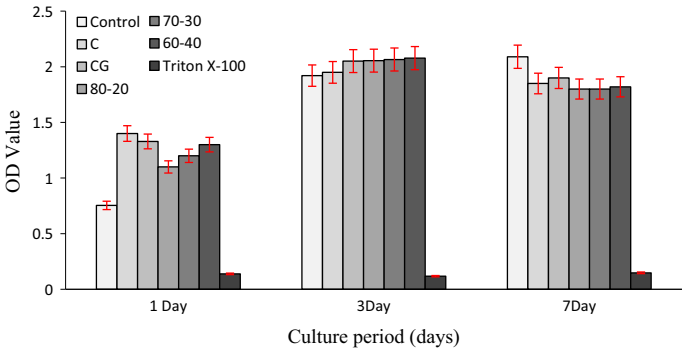

Fig. 10 In vitro cytotoxicity evaluation of MC_3T_3-E_1 cells in contact with scaffolds tracts for different periods of time

related to the composite groups were not like this. The fact that the proliferation of MC_3T_3-E_1 cells is more active along with the CG/nDP nanocomposite scaffolds might be explained by the formation of appropriate active binding sites for proteins during culture periods, resulting in the more efficient induction of cellular proliferation than the control group. MTT results showed that composite scaffolds had a slightly decreased OD value after 24 h; however, after 7 days, no significant difference was seen. This could be due to the low crystallinity of nDP, leading to the dissolution of calcium and phosphate into the media; this, in turn, leads to the increase in intracellular calcium and phosphate concentration, which may induce cell death. The results showed that the composite scaffolds were cytocompatible and no morphological change was observed in MC_3T_3-E_1 cells placed in direct contact with the composite scaffold. Figure 11a, b shows typical scanning electron micrographs of the nanocomposite scaffolds after 14 days of incubation in the cell culture medium alone and after incubation with cells. The higher attachment on nanocomposite scaffolds could be due to the increase in the surface area. It is known that an increase in surface area allows the maximum area for cell attachment and nano-surfaces have a larger surface area to volume ratio [48]. The results indicated

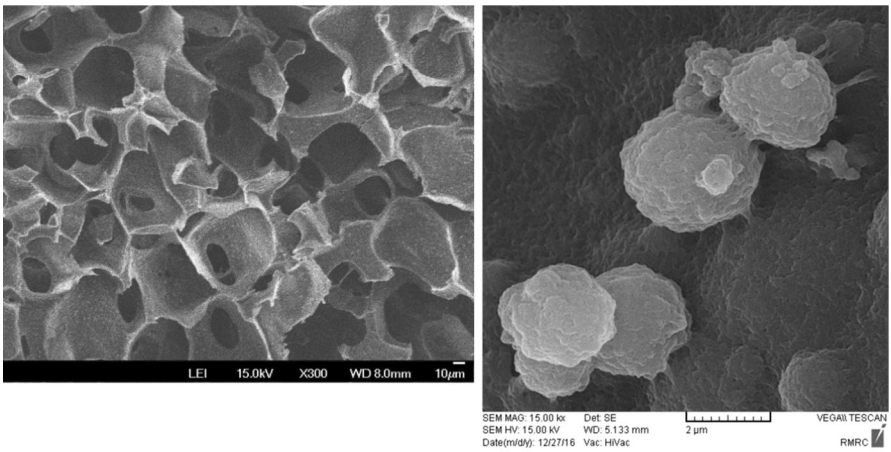

Fig. 11 SEM images of **a** composite CG/nDP 80/20 composite after 14 days in culture medium without cells and **b** cells MC_3T_3-E_1 attached on the scaffolds represents, respectively

that the CG/nDP nanocomposite scaffolds might be suitable for tissue engineering applications.

As previously mentioned, the influence of nDP on CG composite scaffolds prepared through freeze-drying method is not well understood. However, there are several advantages of the freeze-drying method, including use of water and ice crystals instead of an organic solvent in the scaffold fabrication process, which is more suitable for biomedical applications. In this study, by controlling the freeze-drying parameters like pre-freezing temperature and rate of cooling, the available time for the growth of ice crystals expanded. It resulted in bigger pore sizes and at the same time an increased crystallinity [31, 49].

Conclusions

CG/nDP composite scaffolds were synthesized through freeze-drying approach. The resulted scaffolds were characterized and compared together. The composite scaffolds were found to have favorable pore size (150–300 μm) and porosity (70–81%). The mechanical, hydrophilicity and biological characteristics of the scaffolds were influenced by addition of nDP content and changing the ratio of CG in the scaffolds. nDP substantially improved cell attachment on the scaffold surfaces. Thus, nDP played the role of improving biological, cellular behavior and mechanical properties of the scaffolds at the same time. The addition of nDP to CG provided a more promising non-toxic scaffold for tissue engineering applications.

Acknowledgements The authors are grateful to the Payame Noor University in Isfahan Research council (Grant # 62370). The authors would like to thank Dr. L. Ghorbanian for the critical reading of the manuscript, and Mrs. Hydari for providing cell culture facilities.

References

1. Youqing S, Yihong Z, Jianbin T (2008) Multifunctioning pH-responsive nanoparticles from hierarchical self-assembly of polymer brush for cancer drug delivery. Am Inst Chem Eng J 54:2979–2989
2. Vacanti JP, Langer R (1999) Tissue engineering: the design and fabrication of living replacement devices for surgical reconstruction and transplantation. Lancet 354:32–34
3. Hutmacher DW (2000) Scaffolds in tissue engineering bone and cartilage. Biomaterials 21:2529–2543
4. Muzzarelli R, Baldassarre V, Conti F (1988) Biological activity of chitosan: ultrastructural study. Biomaterials 9:247–252
5. Jayakumar R, Prabaharan M, Reis RL (2007) Sulfated chitin and chitosan as novel biomaterials. Int J Biol Macromol 40:175–181
6. Lifeng Q, Zirong X, Xia J (2004) Preparation and antibacterial activity of chitosan nanoparticles. Carbohydr Res 339:2693–2700
7. Muzzarelli RAA (2009) Chitins and chitosans for the repair of wounded skin, nerve, cartilage and bone. Carbohydr Polym 76:167–182
8. Muzzarelli RAA, Giacomelli G (1987) The blood anticoagulant activity of *N*-carboxymethylchitosan trisulfate. Carbohydr Polym 7:87–96
9. Muzzarelli RAA, Tarsi R, Filippini O (1990) Antimicrobial properties of *N*-carboxybutyl chitosan. Antimicrob Agents Chemother 34:2019–2023
10. Mao JS, Zhao LG, Yin YJ (2003) Structure and properties of bilayer chitosan–gelatin scaffolds. Biomaterials 24:1067–1074
11. Lien SM, Ko LY, Huang TJ (2009) Effect of pore size on ECM secretion and cell growth in gelatin scaffold for articular cartilage tissue engineering. Acta Biom 5:670–679
12. Nagahama H, Rani VVD, Shalumon KT (2009) Preparation, characterization, bioactive and cell attachment studies of α-chitin/gelatin composite membranes. Int Biol Macromol 44:333–337
13. Nagahama H, Maeda H, Kashiki T (2009) Preparation and characterization of novel chitosan/gelatin membranes using chitosan hydrogel. Carbohydr Polym 76(2):255–260
14. Mohamed KR, Beherei HH, EL-Rashidy ZM (2014) In vitro study of nano-hydroxyapatite/chitosan–gelatin composites for bio-applications. J Ad Res 5:201–208
15. Kanchan M, Sudip D, Krishna P, Akalabya B (2016) Preparation and evaluation of gelatin–chitosan–nanobioglass 3D porous scaffold for bone tissue engineering. Int J Biomater 2016:1–14
16. Peter M, Ganesh N, Selvamurugan N, Nair SV, Furuike T, Tamura H, Jayakumar R (2010) Preparation and characterization of chitosan–gelatin/nanohydroxyapatite composite scaffolds for tissue engineering applications. Carbohydr Polym 80:687–694
17. Yuji Y, Fen Y, Junfeng C, Fujiang Z, Xiulan L, Kangde Y (2003) Preparation and characterization of macroporous chitosan–gelatin/β-tricalcium phosphate composite scaffolds for bone tissue engineering. J Biomed Mater Res A 67:844–855
18. Huang YC, Chu HW (2013) Using hydroxyapatite from fish scales to prepare chitosan/gelatin/hydroxyapatite membrane: exploring potential for bone tissue engineering. J Mar Sci Tech 21:716–722
19. Wu C, Chang J (2007) Degradation, bioactivity, and cytocompatibility of diopside, akermanite, and bredigite ceramics. J Biom Mat Res Part B Appl Biom 83:153–160
20. Ghomi H, Emadi R, Haghjooye Javanmard S (2016) Preparation of nanostructure bioactive diopside scaffolds for bone tissue engineering by two near net shape manufacturing techniques. Mater Lett 167:157–160
21. Cijun S, Tingting L, Chengde G, Pei F, Shuping P (2014) Mechanical reinforcement of diopside bone scaffolds with carbon nanotubes. Int J Mol Sci 15:19319–19329
22. Chengtie W, Yogambha R, Hala Z (2010) Porous diopside ($CaMgSi_2O_6$) scaffold: a promising bioactive material for bone tissue engineering. Acta Biomater 6:2237–2245
23. Ishu K, Ashutosh G, Dilshat UT, Maria JP, Hye-Young L, Hae-Won K, Jose MFF (2011) Diopside ($CaO{\cdot}MgO{\cdot}2SiO_2$)-fluorapatite ($9CaO{\cdot}3P_2O_5{\cdot}CaF_2$) glassceramics: potential materials for bone tissue engineering. J Mater Chem 21:16247–16256
24. Hosseini Y, Emadi R, Kharaziha M, Doostmohammadi A (2016) Reinforcement of electrospun poly(ε-caprolactone) scaffold using diopside nanopowder to promote biological and physical properties. J Appl Polym Sci 44433:1–9

25. Nonami T, Tsutsumi S (1999) Study of diopside ceramics for biomaterials. J Mater Sci Mater Med 10:475–479
26. Danilchenko SN, Kalinkevich OV, Pogorelov MV (2009) Chitosan–hydroxyapatite composite biomaterials made by a one step co-precipitation method: preparation, characterization and in vivo tests. J Biol Phys Chem 9:119–126
27. Peniche C, Yaimara S, Natalia D (2010) Chitosan/hydroxyapatite-based composites. Biotechnol Appl 27:202–210
28. Yili Q, Danting A, Ping W (2014) Chitosan/nano-hydroxyapatite composite electret membranes enhance cell proliferation and osteoblastic expression in vitro. J Bio Compat Polym 29(1):3–14
29. Zhang X, Liu C, Li M (2009) Fabrication of hydroxyapatite/diopside/alumina composites by hot-press sintering process. Ceram Int 35:1969–1973
30. Zhang MF, Zhang XH, Liu CX (2013) Hydroxyapatite/Al_2O_3/diopside ceramic composites and their behaviour in simulated body fluid. Mater Sci Technol 29:378–382
31. Ghorbanian L, Emadi R, Razavi SM, Shin H, Teimouri A (2013) Fabrication and characterization of novel diopside/silk fibroin nanocomposite scaffolds for potential application in maxillofacial bone regeneration. Int J Biol Macromol 58:275–280
32. Teimouri A, Ghorbanian L, Najafi Chermahini A (2014) Fabrication and characterization of silk/-forsterite composites for tissue engineering applications. Ceram Int 40:6405–6411
33. Teimouri A, Ebrahimi R, Emadi R (2015) Nano-composite of silk fibroin-chitosan/nano ZrO_2 for tissue engineering applications: fabrication and morphology. Int J Biol Macromol 76:292–302
34. Teimouri A, Ebrahimi R, Najafi Chermahini A (2015) Fabrication and characterization of silk fibroin/chitosan/nano γ-alumina composite scaffolds for tissue engineering applications. RSC Adv 5:27558–27570
35. Teimouri A, Azadi M, Emadi R (2015) Preparation, characterization, degradation and biocompatibility of different silk fibroin based composite scaffolds prepared by freeze-drying method for tissue engineering application. Polym Deg Stab 121:18–29
36. Azadi M, Teimouri A, Mehranzadeh G (2016) Preparation, characterization and biocompatible properties of β-chitin/silk fibroin/nanohydroxyapatite composite scaffolds prepared by freeze-drying method. RSC Adv 6:7048–7060
37. Ghorbanian L, Emadi R, Teimouri A (2012) Synthesis and characterization of novel nanodiopsidebioceramic powder. JNS 2:357–361
38. Nazarov R, Jin HJ, Kaplan DL (2004) Porous 3-D scaffolds from regenerated silk fibroin. Biomacromol 5:718–726
39. Rockwood DN, Preda RC, Yucel T (2011) Materials fabrication from bombyx mori silk fibroin. Nat Prot 10:1612–1631
40. Li J, Dou Y, Yang J (2009) Surface characterization and biocompatibility of micro- and nano-hydroxyapatite/chitosan–gelatin network films. Mater Sci Eng C 29:1207–1215
41. Teimouri A, Azadi M (2016) Preparation and characterization of novel chitosan/nanodiopside/nanohydroxyapatite composite scaffolds for tissue engineering applications. Int J Polymer Mater Polymer Biomater 65:917–927
42. Teimouri A, Azadi M, Shams Ghahfarokhi Z, Razavizadeh R (2016) Preparation and characterization of novel β-chitin/nanodiopside/nanohydroxyapatite composite scaffolds for tissue engineering applications. J Biomater Sci Polym Ed 28:1–14
43. Teimouri A, Azadi M (2016) β-Chitin/gelatin/nanohydroxyapatite composite scaffold prepared through freeze-drying method for tissue engineering applications. Polym Bull 73:3513–3529
44. Padilla S, Roman J, Sanchez-Salcedo S (2006) Hydroxyapatite/SiO_2–CaO–P_2O_5 glass materials: in vitro bioactivity and biocompatibility. Acta Biomater 3:331–342
45. Kokubo T (1991) Bioactive glass ceramics: properties and applications. Biom 2:155–163
46. Lluch V, Ferrer GG, Pradas MM (2009) Biomimetic apatite coating on P(EMA-co-HEA)/SiO_2 hybrid nanocomposites. Polym 50:2874–2884
47. Tanahashi M, Yao T, Kokubo T (1994) Apatite coating on organic polymers by a biomimetic process. J Am Ceram Soc 77:2805–2808
48. Blaker J, Gough J, Maquet V (2003) In vitro evaluation of novel bioactive composites based on Bioglass®-filled polylactide foams for bone tissue engineering scaffolds. J Biom Mat Res Part A 67:1401–1411
49. Lu T, Li Y, Chen T (2013) Techniques for fabrication and construction of three-dimensional scaffolds for tissue engineering. Int J Nanomed 8:337–350